DOI:10.1021/jf101531c

JOURNAL OF AGRICULTURAL AND FOOD CHEMISTRY
ARTICLE

Direct Electrochemical Determination of Methyl Jasmonate in Wheat Spikelet at a Nano-Montmorillonite Film Modified Electrode by Derivative Square Wave Voltammetry

Tian Gan,[†] Chengguo Hu,[†] Zilin Chen,[‡] and Shengshui Hu*[,†,§]

[†]Key Laboratory of Analytical Chemistry for Biology and Medicine (Ministry of Education), College of Chemistry and Molecular Sciences, and [‡]Department of Pharmaceutical Analysis, College of Pharmacy, Wuhan University, Wuhan 430072, People's Republic of China, and [§]State Key Laboratory of Transducer Technology, Chinese Academy of Sciences, Beijing 10080, People's Republic of China

The direct electrochemical determination of methyl jasmonate (MeJA) at a nano-montmorillonite modified glassy carbon electrode (nano-MMT/GCE) is reported. The modified electrode, prepared by a simple casting−drying method and characterized by scanning electron microscope (SEM) and electrochemical impedance spectra (EIS), was proved to process a uniform nanostructured surface with a large surface area and a fast electron transfer rate. This electrode exhibited a sensitive electrochemical response for the direct oxidation of MeJA in 0.1 mol L^{-1} $HClO_4$, which could be further improved by using a derivative square wave voltammetry technique. Thus, a simple and fast electrochemical method for the determination of MeJA is proposed. Under optimal working conditions, the oxidation current of MeJA linearly increased with its concentration in the range of 7.0×10^{-7}−1.0×10^{-3} mol L^{-1} with a detection limit of 5.0×10^{-7} mol L^{-1}. This method had been applied to the determination of MeJA content in wheat spikelet samples.

KEYWORDS: Methyl jasmonate; nano-montmorillonite; electrochemical determination; derivative voltammetry

INTRODUCTION

Methyl jasmonate (MeJA), a plant regulator compound, exists naturally in a wide range of higher plants. MeJA is known to regulate a number of physiological processes in plants, including the induction of proteinase inhibitors, meristematic growth, senescence, vegetative storage proteins, and interplant signals (*1*). MeJA is also involved in signal transduction, especially in relation to defense gene activation (*2*, *3*). Recently, MeJA has been successfully applied to induce or increase the biosyntheses of many important secondary metabolites in plant cells (*4*,*5*). Owing to its important physiological roles and the rather low content in plants, a variety of chromatographic methods were carried out for the determination of MeJA, for example, gas chromatography (*6*, *7*), reverse-phase capillary liquid chromatography (*8*), and online coupling of reversed-phase liquid chromatography to gas chromatography (*9*). The detectors employed in these methods are usually confined to mass spectrometry (MS) (*6*−*8*), ultraviolet−visible spectrophotometry (UV−vis) (*9*), and flame ionization detectors (FID) (*7*, *9*).

Electrochemical methods, with the merits of low cost, easy operation, fast response, and high sensitivity, have been widely used for the determination of various phytohormones, such as indole-3-acetic acid (*10*−*12*), abscisic acid (*13*), gibberellin acid (*14*), and salicylic acid (*15*−*17*). To our knowledge, no electrochemical methods for the determination of MeJA have been reported, due to its poor electroactivity.

Montmorillonite (MMT), a kind of natural nonmetallic mineral, has two tetrahedral layers and one octahedral layer bonded together with cations in the sheets. The colloidal MMT films on electrode surface with flexible adsorptive properties and good penetrability, can provide a favorable microenvironment for electron transfer between analytes and electrodes and, therefore, can be used as catalysts or catalytic supports for many substances, such as methylparathion (*18*), H_2O_2 (*19*), cytochrome (*20*), and analgesics (*21*). The utilization of clay-modified electrodes for electroanalytical applications has been summarized by Walcarius (*22*).

In this work, a simple electrochemical method based on the first-order derivative square wave voltammetry (first SWV) for the direct determination of MeJA at a nano-montmorillonite film modified glassy carbon electrode (nano-MMT/GCE) was proposed. Several techniques, such as scanning electron microscope (SEM), electrochemical impedance spectra (EIS), and chronocoulometry, were employed for characterizing the surface morphology and interface property of the electrode, as well as the electrochemical behavior of MeJA at the nano-MMT/GCE. The results indicated that the high surface area of nano-MMT/GCE, along with the fast electron and mass transfer rate of MeJA at this electrode, was responsible for the enhanced oxidation response of MeJA. The successful determination of MeJA content in wheat spikelet by this method foresaw its promising application in the fast determination of MeJA and its analogues in real plant samples.

*Corresponding author (fax +86-27-6875 4067; phone +86-27-8788 1642; e-mail sshu@whu.edu.cn).

 Published on Web 07/22/2010

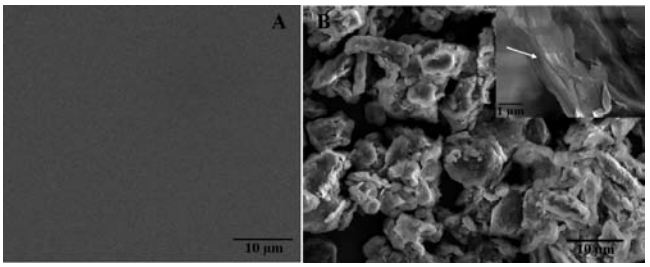

Figure 1. SEM images of GCE (**A**) and nano-MMT film modified GCE (**B**). (Inset of **B**) Lateral image of nano-MMT film on GCE.

EXPERIMENTAL PROCEDURES

Reagents and Solutions. Nano-sodium montmorillonite (~25 nm) was purchased from the Fenghong Clay Chemicals Co., Ltd. (Zhejiang, China). The content of montmorillonite was 96−98%, and the apparent density and diameter thickness ratio of the material were 0.25−0.35 g cm^{-3} and 200, respectively. MeJA was purchased from Sigma-Aldrich, Germany. A 0.1 mol L^{-1} stock solution of MeJA was prepared with methanol and stocked in darkness at 4 °C, which was further diluted to desired concentrations by methanol. All chemicals were of analytical reagent grade and used without further purification.

Apparatus. All electrochemical measurements were carried out on a CHI 830B electrochemical analyzer (Shanghai Chenhua Co., China). A conventional three-electrode system, including a nano-MMT film modified electrode (3 mm in diameter), a saturated calomel reference electrode (SCE), and a platinum wire auxiliary electrode, was employed.

Electrochemical impedance spectroscopy (EIS) was carried out on an EG&G model 273 electrochemical workstation and an EG&G model 5210 lock-in amplifier (Princeton Applied Research, PAR, USA) powered by Echem software.

SEM images were obtained on a Sirion 200 field scanning electron microscope (FEI, Holland).

Preparation of the Modified Electrode. A glassy carbon electrode (GCE) was first polished with 0.05 μm alumina slurry on silk and then washed with ethanol/water (1:1) and double-distilled water in an ultrasonic bath, each for 1 min.

Suspension of nano-MMT was prepared by vigorously stirring 20.0 mg of nano-MMT in 10.0 mL of redistilled water for 48 h. The clay suspension was then centrifuged at 5000 rpm for 20 min, and the supernatant was collected. The obtained nano-MMT colloid was stocked at 4 °C when not in use and was stable against flocculation for several months.

For preparing nano-MMT/GCE, 10.0 μL of the resulting nano-MMT colloid was coated onto the surface of GCE and allowed to dry under an infrared lamp in the air.

Experimental Procedure. Unless otherwise stated, a 0.1 mol L^{-1} $HClO_4$ solution was used as the supporting electrolyte for the determination of MeJA. The SW voltammograms were recorded from 1.25 to 1.80 V after 60 s of accumulation, and the voltammetric curves were treated with the first-derivative technique on a CHI-830 electrochemical workstation.

Extraction of MeJA from Spikelets of Wheat. The wheat spikelet samples were obtained from Jiangxi Agricultural University China. They were frozen in liquid nitrogen from the moment they were picked up and lyophilized. A portion of 0.5 g of spikelte samples was then ground to fine powder in a mortar using a pestle, collected in a vessel, and mixed with 35.0 mL of methanol for overnight extraction in a refrigerator. The supernatant was collected after centrifugation at 12000 rpm for 20 min.

RESULTS AND DISCUSSION

Surface Morphology of Nano-MMT/GCE. The surface morphology of the nano-MMT/GCE is characterized by SEM images (**Figure 1**). Compared with the rather smooth surface of GCE (**A**), a uniform and compact film comprising folded MMT nanoparticles and many nanopores is observed at nano-MMT/GCE (**B**), which is made up of layered nanostructure of MMT as indicated in the inset of **Figure 1B**. These can not only improve the effective surface area of the electrode because of the nanostructure of MMT film but also create plenty of electroactive/adsorption sites for analytes by the ion exchange capacity of MMT.

Electrochemical Property of Nano-MMT/GCE. Electrochemical impedance spectrometry (EIS) is a powerful tool for exploring the interface property of chemically modified electrodes. **Figure 2A** shows the EIS results of 5 mmol L^{-1} $K_3Fe(CN)_6$ (in 0.1 mol L^{-1} KCl) at GCE (a) and nano-MMT/GCE (b). The EIS spectra include a semicircular part at high frequencies and a linear part at low frequencies, corresponding to the electron transfer process and the diffusion process, respectively. The semicircle of nano-MMT/GCE with a much smaller diameter indicates a faster electron transfer rate between $K_3Fe(CN)_6$ and the electrode surface when the surface of GCE is modified by nano-MMT. Therefore, the nano-MMT film on GCE can greatly increase the electron transfer rate, probably due to the nanostructured surface property of the nano-MMT film. The electrochemical behaviors of 5 mmol L^{-1} $K_3Fe(CN)_6$ at GCE (a′) and nano-MMT/GCE (b′) are shown in **Figure 2B**. $K_3Fe(CN)_6$ possesses lower redox currents on the nano-MMT modified GCE but with a smaller peak-to-peak separation. The much lower redox current of $K_3Fe(CN)_6$ at MMT/GCE is due to the electrostatic repulsion of $K_3Fe(CN)_6$ at the negatively charged MMT film (*23*), whereas the apparently smaller peak-to-peak separation may arise from the facilitated electron transfer of $K_3Fe(CN)_6$ at the pinholes or cracks in the MMT film as indicated by the SEM image (**Figure 1B**), according with the EIS behaviors of GCE and nano-MMT/GCE.

Figure 3 shows the cyclic voltammograms of GCE (a) and nano-MMT/GCE (b) in 0.1 mol L^{-1} NaCl containing 5 mmol L^{-1} $Ru(bpy)_3^{2+}$. In comparison to the poor signal at GCE, the redox peaks of $Ru(bpy)_3^{2+}$ are apparently improved, due to the strong adsorption capacity of nano-MMT for positively charged $Ru(bpy)_3^{2+}$ (*23*). From the redox peaks of $Ru(bpy)_3^{2+}$ at these two electrodes, the effective electrode surface area (A_e) can be calculated according to the Randles−Sevcĭk equation

$$I_p = (2.687 \times 10^5) n^{3/2} A_e D^{1/2} c \nu^{1/2} \quad (1)$$

where n is the number of electrons transferred, D is the diffusion coefficient, c is the bulk concentration, and ν is the scan rate. From the inset of **Figure 3**, it can be seen that the plot of peak current of $Ru(bpy)_3^{2+}$ (I_p) changes linearly with $\nu^{1/2}$ at GCE (a′) and nano-MMT/GCE (b′). Comparison of the slopes of the two electrodes reveals that A_e of nano-MMT film modified GCE is 5.4-fold larger than that of GCE, which shows that the formation of MMT nanostructures on GCE can obviously enlarge the surface area.

Electrochemical Behavior of MeJA at the Nano-MMT/GCE. The voltammetric behaviors of MeJA at GCE and nano-MMT/GCE are studied (**Figure 4**). Only an oxidation peak of 3.0×10^{-3} mol L^{-1} MeJA at both GCE (a) and nano-MMT/GCE (b) can be seen, which indicates that the oxidation of MeJA is totally irreversible. Moreover, the oxidation current gradually decreased with increasing potential sweep loop (not shown), possibly as a result of the irreversible strong adsorption of electrochemically inert product on the electrode surface. Thus, the first scan was collected in the following experiments. Compared with GCE, the peak current increases greatly at nano-MMT/GCE, suggesting the enhanced accumulation of MeJA by nano-MMT film with a large surface area.

The SW voltammetric responses of 5.5×10^{-4} mol L^{-1} MeJA in 0.1 mol L^{-1} $HClO_4$ at GCE and nano-MMT/GCE are shown in **Figure 4A**. Obviously, a sensitive oxidation peak appears at nano-MMT/GCE (e), whereas only a small one is observed at GCE (c). This, coupled with the SW voltammogram of nano-MMT/GCE in 0.1 mol L^{-1} $HClO_4$ (d), suggests that the peak at

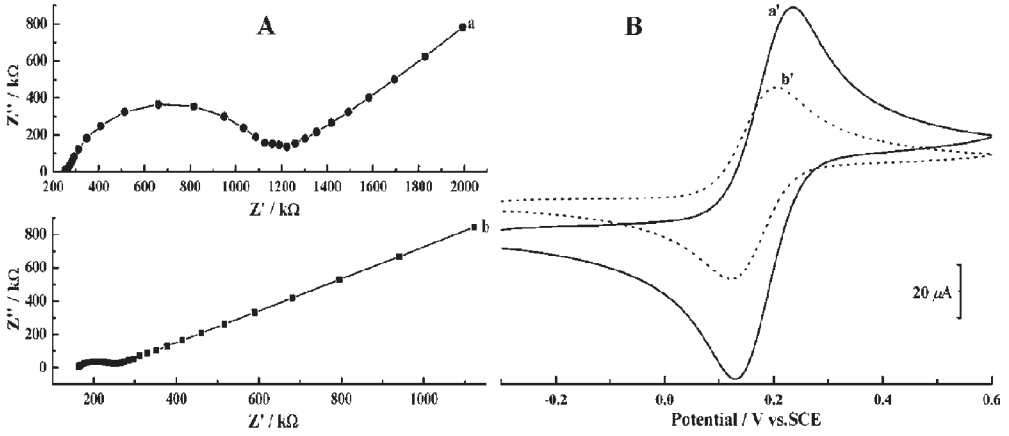

Figure 2. (**A**) Nyquist diagram (Z'' vs Z') for the EIS measurements in the presence of 5 mmol L^{-1} $K_3Fe(CN)_6$ in 0.1 mol L^{-1} KCl at GCE (a) and nano-MMT/GCE (b). (**B**) Cyclic voltammograms of 5 mmol L^{-1} $K_3Fe(CN)_6$ in 0.1 mol L^{-1} KCl at GCE (a′) and nano-MMT/GCE (b′) with a scan rate of 100 mV s^{-1}.

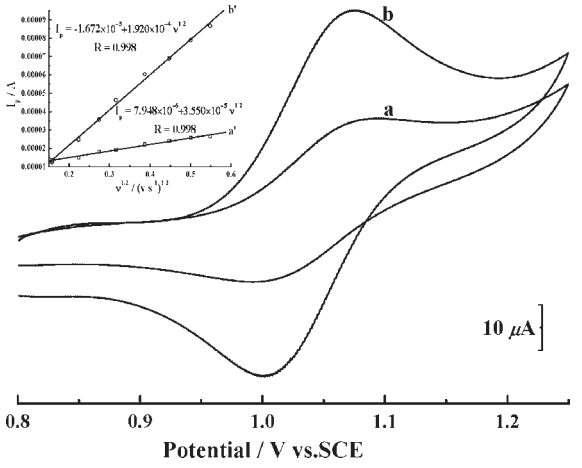

Figure 3. Cyclic voltammograms of 5 mmol L^{-1} $Ru(bpy)_3^{2+}$ in 0.1 mol L^{-1} NaCl at GCE (a) and nano-MMT/GCE (b) with a scan rate of 100 mV s^{-1}. (Inset) Influence of scan rate on the peak current of $Ru(bpy)_3^{2+}$.

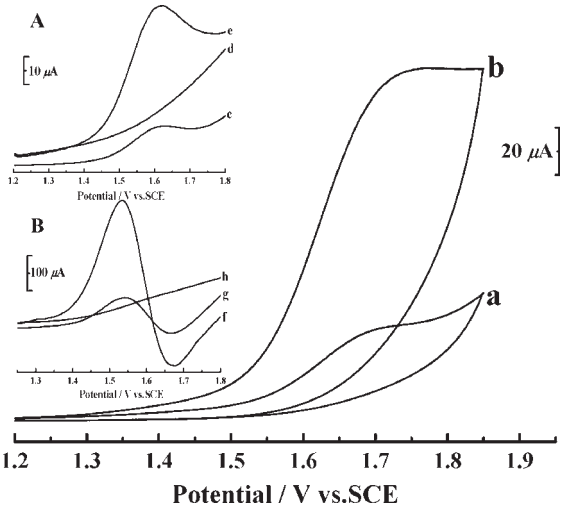

Figure 4. CVs of 3.0 × 10^{-3} mol L^{-1} MeJA at bare GCE (a) and nano-MMT/GCE (b) in 0.1 mol L^{-1} $HClO_4$. Scan rate = 100 mV s^{-1}. (**A**) SWV behaviors of 5.5 × 10^{-4} mol L^{-1} MeJA at GCE (c), nano-MMT/GCE (e). (**B**) First SWV behaviors of 5.5 × 10^{-4} mol L^{-1} MeJA at GCE (g), nano-MMT/GCE (f). d and h correspond to the SWV and first SWV curves of nano-MMT/GCE in 0.1 mol L^{-1} $HClO_4$, respectively. Pulse height = 25 mV, pulse width = 40 ms.

1.60 V is attributed to the oxidation of MeJA. Because the major hindrance of the electrochemical determination of MeJA is the poor electroactivity of MeJA that produces a weak voltammetric signal, the method of first-order derivative square voltammetry (first SWV) is utilized here considering its function to extract the signals from background (*24*). As shown in **Figure 4B**, the oxidation peaks become much sharper at both nano-MMT/GCE (f) and GCE (g) through first-derivative processing. The sensitivity for MeJA determination can be improved to a large extent, and the derivative technique is also applied to curve d (h), which further proves the right oxidation peak of MeJA.

Oxidation Mechanism of MeJA. In 0.1 mol L^{-1} $HClO_4$ solution, the oxidation responses of 5.0 × 10^{-4} mol L^{-1} MeJA at different scan rates are investigated using linear sweep voltammetry (LSV). As the scan rate increases from 25 to 400 mV s^{-1}, the oxidation peak current (I_p) of MeJA increases linearly, suggesting that the oxidation of MeJA at nano-MMT/GCE is controlled by adsorption. For the irreversible surface electrochemical reaction, the relationship between the peak potential E_p and the scan rate ν can be expressed as (*25*)

$$E_p = E^{0'} + \left(\frac{RT}{\alpha nF}\right) \ln\left(\frac{RTk^0}{\alpha nF}\right) + \left(\frac{RT}{\alpha nF}\right) \ln \nu \qquad (2)$$

where k^0 is the standard rate constant of the surface reaction, $E^{0'}$ is the formal potential, and other symbols have their usual meanings.

According to eq 2, the plot of E_p versus ln ν has a good linear relationship, from which αn can be determined from the slope (calcd 0.0273) and k^0 can be calculated from the intercept if the value of $E^{0'}$ is known. Here, the value of $E^{0'}$ is deduced from the intercept of E_p versus ν by extrapolating the vertical axis to $\nu = 0$ as 1.4439 V. Thus, the values of $\alpha n = 0.94$ and $k^0 = 1.23$ s^{-1} are calculated. Assuming $\alpha = 0.5$, two electrons are involved in the totally irreversible oxidation of MeJA.

To further explore the electrochemical oxidation mechanism of MeJA at MMT/GCE, a comparison experiment is performed between MeJA and its structural analogue, methyl dihydrojasmonate (DH-MeJA) (**Figure 5**). In constrast to the well-defined oxidation peak of MeJA (curve a), no any redox peaks are observed for DH-MeJA. Therefore, the oxidation of MeJA may occur at its alkene group.

Chronocoulometry. Chronocoulometry is used to characterize the oxidation of 5.0 × 10^{-4} mol L^{-1} MeJA on nano-MMT/GCE (**Figure 6**, a) and GCE (**Figure 6**, b) in 0.1 mol L^{-1} $HClO_4$. The diffusion coefficient (D) and Faradaic charge due to the oxidation of adsorbed MeJA (Q_{ads}) in these two systems can be obtained

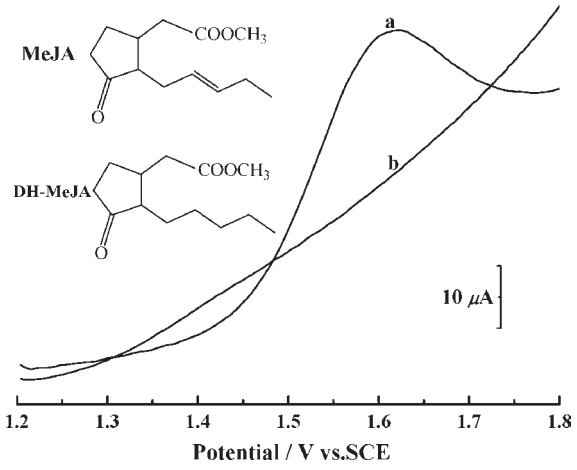

Figure 5. SW voltammograms of 5.5×10^{-4} mol L^{-1} MeJA (a) and DH-MeJA (b) in 0.1 mol L^{-1} $HClO_4$. SWV conditions are as in **Figure 4**.

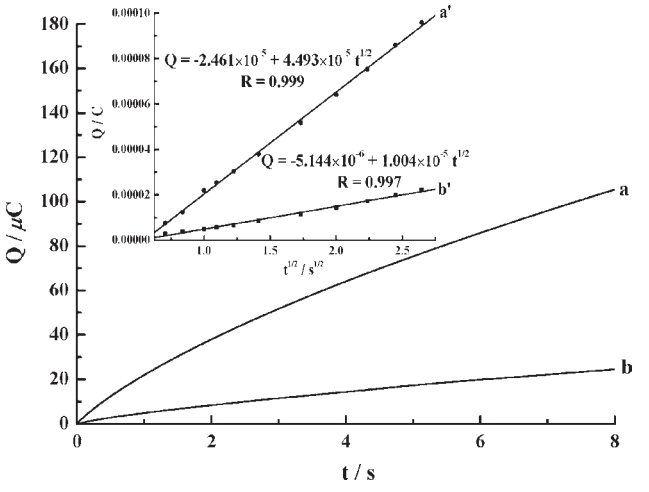

Figure 6. Chronocoulometry and the linear relationships between charge and the square root of time for 5.0×10^{-4} mol L^{-1} MeJA in 0.1 mol L^{-1} $HClO_4$ at nano-MMT/GCE (a, a′) and bare GCE (b, b′). The initial potential is 1.68 V, the final potential is 1.78 V, and the pulse width is 8 s.

according to Anson's equation (*26*)

$$Q = \frac{2nFA_a cD^{1/2}}{\pi^{1/2}} t^{1/2} + Q_{dl} + Q_{ads} \quad (3)$$

where c is the concentration of MeJA, Q_{dl} is the double-layer charge, A_a is the apparent electrode surface area, and other symbols are as usual. The subtraction of the background charge can eliminate the effect of the double-layer charge, Q_{dl}. Here, $n = 2$, $c = 5.0 \times 10^{-4}$ mol L^{-1}, $A_a = 0.0707$ cm^2, and the slope values are 10.04 and 44.93 μC $s^{-1/2}$ for GCE (inseted curve b′) and nano-MMT/GCE (inseted curve a′), respectively. The calculated values of 1.70×10^{-6} and 3.40×10^{-5} cm^2 s^{-1} for D and the values of 24.61 and 51.44 μC for Q_{ads} at GCE and nano-MMT/GCE can be obtained, respectively. According to the following equation

$$Q_{ads} = nFA\Gamma \quad (4)$$

the surface coverage (Γ) is 7.62×10^{-10} and 1.35×10^{-9} mol cm^{-2} for GCE and nano-MMT/GCE, respectively. These demonstrate the stronger accumulation capacity of nano-MMT/GCE compared with GCE for the adsorption of MeJA.

Detection of MeJA at Nano-MMT/GCE. The electrochemical responses of 3.0×10^{-4} mol L^{-1} MeJA at nano-MMT/GCE in

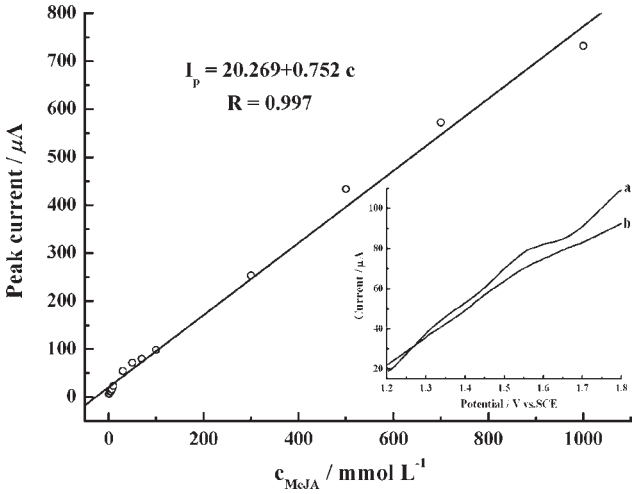

Figure 7. Calibration graph for the determination of MeJA at nano-MMT/GCE in 0.1 mol L^{-1} $HClO_4$. (Inset) First SW voltammograms of nano-MMT/GCE in 5.0×10^{-7} mol L^{-1} MeJA (a) and 0.1 mol L^{-1} $HClO_4$ (b). SWV conditions are as in **Figure 4**.

different supporting electrolytes, such as 0.1 mol L^{-1} phosphate buffer solution (pH 5.0−8.0), sodium acetate−acetic acid buffer solution (pH 2.6−5.0), NaOH, HCl, H_2SO_4, and $HClO_4$ are examined using SWV. It is found that the peak current of MeJA was the largest and the peak shape was the best in 0.1 mol L^{-1} $HClO_4$. Thus, 0.1 mol L^{-1} $HClO_4$ was selected as the suitable electrolyte for the electrochemical detection of MeJA.

The influence of modifier content (volume) on the oxidation peak current of 3.0×10^{-4} mol L^{-1} MeJA in 0.1 mol L^{-1} $HClO_4$ was studied (figure not shown). Generally, the oxidation current increases quickly with the increase of modifier volume in the range of 0.0−10.0 μL. However, further improving the volume of nano-MMT suspension leads to the decrease of oxidation peak current lightly, due to the block of electron transfer by a too-thick MMT film. As a result, 10.0 μL of nano-MMT suspension was suitable for the fabrication of nano-MMT film modified electrode.

To evaluate the influence of accumulation potential on the determination of MeJA, the oxidation peak currents of 3.0×10^{-4} mol L^{-1} MeJA for an accumulation period of 60 s under different accumulation potentials were measured. It is found that the oxidation peak current changes slightly with accumulation potential. Thus, the accumulation step was performed at the initial potential for convenience. The influence of accumulation time on the oxidation current of 3.0×10^{-4} mol L^{-1} MeJA is also examined (figure not shown), which shows that the peak current increases almost linearly with the accumulation time in the range of 0−60 s. When the accumulation time is further increased to 180 s, the peak current changes slowly and tends to be stable, due to the saturation of surface coverage of MeJA on the electrode surface. An accumulation time of 60 s was employed in the following measurement.

Calibration and Anti-interference Capacity. Under the optimal working conditions, the calibration plot for MeJA in 0.1 mol L^{-1} $HClO_4$ at nano-MMT/GCE is characterized by first SWV. The oxidation current of MeJA linearly increases with its concentration in the range of 7.0×10^{-7}−1.0×10^{-3} mol L^{-1}, and the detection limit is 5.0×10^{-7} mol L^{-1} for an accumulation period of 60 s (**Figure 7**). Because the adsorption of MeJA at the nano-MMT film is strong, it is necessary to construct a new film after each analysis. The relative standard deviation (RSD) is 2.9% for the parallel measurements of 3.0×10^{-4} mol L^{-1} MeJA at 10 electrodes, suggesting that this method possesses good reproducibility.

Table 1. Influences of Other Compounds on the Peak Current of 1.0×10^{-5} mol L^{-1} MeJA

interferent	concentration (mol L^{-1})	signal change (%)
gibberellin	5.0×10^{-3}	−1.31
methyl dihydrojasmonate	5.0×10^{-3}	0.29
indole-3-acetic	5.0×10^{-4}	−4.42
abscisic acid	1.0×10^{-4}	6.34
jasmone	1.0×10^{-4}	7.31
sucrose	5.0×10^{-3}	0.34
glucose	5.0×10^{-3}	3.22
oleic acid	5.0×10^{-3}	−0.22
ricinoleic acid	5.0×10^{-3}	1.37
soluble starch	1.0×10^{-3}	−3.56
SO_4^{2-}	5.0×10^{-3}	−0.96
PO_4^{3-}	5.0×10^{-3}	−2.13
Mg^{2+}	5.0×10^{-4}	4.07
Fe^{2+}	2.0×10^{-4}	5.83
CO_3^{2-}	2.0×10^{-4}	3.21
Fe^{3+}	1.5×10^{-4}	4.95
Ca^{2+}	1.5×10^{-4}	5.74

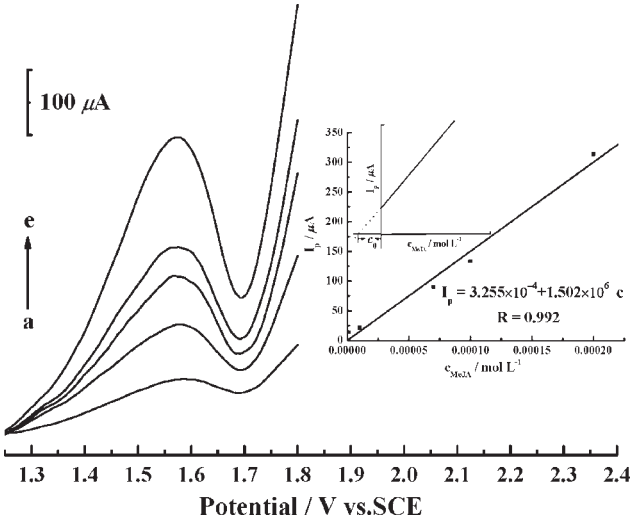

Figure 8. First SW voltammograms obtained in samples spiked with 1.0×10^{-6}, 1.0×10^{-5}, 7.0×10^{-5}, 1.0×10^{-4}, and 2.0×10^{-4} mol L^{-1} MeJA from a to e in 0.1 mol L^{-1} $HClO_4$. (Inset) Calibration graph using extrapolation method. SWV conditions are as in **Figure 4**.

Various possible interferents are tested to assess their influences on the determination of MeJA (**Table 1**). Inteference studies are conducted by exposing nano-MMT/GCE to MeJA in 0.1 mol L^{-1} $HClO_4$ containing interferents at certain concentrations. The results show that 500-fold SO_4^{2-}, PO_4^{3-}, sucrose, glucose, oleic acid and ricinoleic acid, 100-fold soluble starch, 50-fold Mg^{2+}, 20-fold Fe^{2+} and CO_3^{2-}, and 15-fold Fe^{3+} and Ca^{2+} do not interfere with the current response of 1.0×10^{-5} mol L^{-1} MeJA. The interferences of some common phytohormones are also tested. 500-fold gibberellin, methyl dihydrojasmonate, 50-fold indole-3-acetic, and 10-fold abscisic acid and jasmone exert no interference on the current response of 1.0×10^{-5} mol L^{-1} MeJA (signal change below 8.0%). From these data, it seems that this method can be applicable to real plant samples.

Sample Analysis. Considering the rather low content of MeJA in wheat spikelet samples (ususlly 10−1500 ng g^{-1}) (*8*), an extrapolation method was used in our experiment as Watkins et al. did for the determination of chloride in polluted water (*27*). Briefly, five methanol extracts of spikelets (1.0 mL) were spiked with increasing concentrations of standard MeJA from 1.0×10^{-6} to 2.0×10^{-4} mol L^{-1}, and the first SW voltammograms were recorded (**Figure 8**). As expected, a good linear relationship can be obtained between the peak current of MeJA and its concentration (inset of **Figure 8**). To make the data more accurate, an additional five calibration plots were carried out under the same working conditions with different MeJA standard solutions spiked. The initial MeJA value in the spikelet samples (c_0) can be obtained from the intercept of plot I_p versus c_{MeJA} by extrapolation to the vertical axis at $I_p = 0$. The average c_0 value calculated from the six calibration graphs is 37.63 ng g^{-1} (RSD = 5.01%). Furthermore, the good recovery between 99.73 and 106.11% implies a good reliability of this method for real sample analysis. The value c_0 obtained from our method is compared with that from the HPLC method, which is 38.98 ng g^{-1} on average, close to the c_0 data from the electrochemical method, which proves the feasibility of this newly developed method in MeJA detection.

Conclusion. In this work, a new method based on a nano-MMT film modified glassy carbon electrode was first developed for studying the direct electrochemical oxidation of methyl jasmonate. The super characteristics of nano-MMT, such as large surface area, strong adsorptive ability, rich active sites, and subtle electronic properties can improve the sensitivity to detect methyl jasmonate. This method has been successfully applied to determine the concentration of methyl jasmonate in spikelets of wheat samples, foreseeing its promising application as a simple, convenient, and fast electrochemical route for the determination of methyl jasmonate in real samples.

LITERATURE CITED

(1) de Bruxelles, G. L.; Roberts, M. R. Signals regulating multiple responses to wounding and herbivores. *Crit. Rev. Plant Sci.* **2002**, *20*, 487–521.

(2) Farmer, E. E.; Ryan, C. A. Octadecanoid precursors of jasmonic acid activate the synthesis of wound-inducible proteinase inhibitors. *Plant Cell* **1992**, *4*, 129–134.

(3) Wasternack, C. Jasmonates: an update on biosynthesis, signal transduction and action in plant stress response, growth and development. *Ann. Bot.* **2007**, *100*, 681–697.

(4) Zhong, J. J.; Yue, C. J. Plant cells: secondary metabolite heterogeneity and its manipulation. *Adv. Biochem. Eng./Biotechnol.* **2005**, *100*, 53–88.

(5) Hu, F. X.; Zhong, J. J. Jasmonic acid mediates gene transcription of ginsenoside biosynthesis in cell cultures of *Panax notoginseng* treated with chemically synthesized 2-hydroxyethyl jasmonate. *Process Biochem.* **2008**, *43*, 113–118.

(6) Creelman, R. A.; Tierney, M. L.; Mullet, J. E. Jasmonic acid/methyl jasmonate accumulate in wounded soybean hypocotyls and modulate wound gene expression. *Proc. Natl. Acad. Sci. U.S.A.* **1992**, *89*, 4938–4941.

(7) Meyer, R.; Rautenbach, G. F.; Dubery, I. A. Identification and quantificatiom of methyl jasmonate in leaf volatiles of Arabidopsis thaliana using solid-phase microextraction in combination with gas chromatography and mass spectrometry. *Phytochem. Anal.* **2003**, *14*, 155–159.

(8) Wilbert, S. M.; Ericsson, L. H.; Gordon, M. P. Quantification of jasmonic acid, methyl jasmonate, and salicylic acid in plants by capillary liquid chromatography electrospray tandem mass spectrometry. *Anal. Biochem.* **1998**, *257*, 186–194.

(9) Flores, G.; Blanch, G. P.; del Castillo, M. L. R. Through oven transfer adsorption-desorptiom interface for the analysis of methyl jasmonate in aromatic samples by on-line RPLC-GC. *J. Sep. Sci.* **2008**, *31*, 1207–1214.

(10) de Toledo, R. A.; Vaz, C. M. P. Use of a graphite-polyurethane composite electrode for electroanalytical determination of indole-3-acetic acid in soil samples. *Microchem. J.* **2007**, *86*, 161–165.

(11) Wu, K. B.; Sun, Y. Y.; Hu, S. S. Development of an amperometric indole-3-acetic acid sensor based on carbon nanotubes film coated glassy carbon electrode. *Sens. Actuators B: Chem.* **2003**, *96*, 658–662.

(12) Zhang, S. H.; Wu, K. B. Square wave voltammetric determination of indole-3-acetic acid based on the enhancement effect of anionic surfactant at the carbon paste electrode. *Bull. Korean Chem. Soc.* **2004**, *25*, 1321–1325.
(13) Hernández, P.; Dabrio-Ramos, M.; Patón, F.; Ballesteros, Y.; Hernández, L. Determination of abscisic acid by cathodic stripping square wave voltammetry. *Talanta* **1997**, *44*, 1783–1792.
(14) Li, J.; Xiao, L. T.; Zeng, G. M.; Huang, G. H.; Shen, G. L.; Yu, R. Q. Immunosensor for rapid detection of gibberellin acid in the rice grain. *J. Agric. Food Chem.* **2005**, *53*, 1348–1353.
(15) Wang, Z.; Ai, F.; Xu, Q.; Yang, Q.; Yu, J. H.; Huang, W. H.; Zhao, Y. D. Electrocatalytic activity of salicylic acid on the platinum nanoparticles modified electrode by electrochemical deposition. *Colloid surf. B: Biointerfaces* **2010**, *76*, 370–374.
(16) Wang, Z.; Wei, F.; Liu, S. Y.; Xu, Q.; Huang, J. Y.; Dong, X. Y.; Yu, J. H.; Yang, Q.; Zhao, Y. D.; Chen, H. Electrocatalytic oxidation of phytohormone salicylic acid at copper nanoparticles-modified gold electrode and its detection in oilseed rape infected with fungal pathogen *Sclerotinia sclerotiorum*. *Talanta* **2010**, *80*, 1277–1281.
(17) Batchelor-McAuley, C.; Wildgoose, G. G. The influence of substrate effects when investigating new nanoparticle modified electrodes exemplified by the electroanalytical determination of aspirin on NiO nanoparticles supported on graphite. *Electrochem. Commun.* **2008**, *10*, 1129–1131.
(18) Tcheumi, H. L.; Tonle, I. K.; Ngameni, E.; Walcarius, A. Electrochemical analysis of methylparathion pesticide by a gemini surfactant-intercalated clay-modified electrode. *Talanta* **2010**, *81*, 972–979.
(19) Lei, C. H.; Deng, J. Q. Hydrogen peroxide sensor based on co-immobilized methylene green and horseradish peroxidase in the same montmorillonite-modified bovine serum albumin−glutaraldehyde matrix on a glassy carbon electrode surface. *Anal. Chem.* **1996**, *68*, 3344–3349.
(20) Shumyantseva, V. V.; Ivanov, Y. D.; Bistolas, N.; Scheller, F. W.; Archakov, A. I.; Wollenberger, U. Direct electron transfer of cytochrome P450 2B4 at electrodes modified with nonionic detergent and colloid clay nanoparticles. *Anal. Chem.* **2004**, *76*, 6046–6052.
(21) Muralidharan, B.; Gopu, G.; Vedhi, C.; Manisankar, P. Voltammetric determination of analogesics using a montmorillonite modified electrode. *Appl. Clay Sci.* **2008**, *42*, 206–213.
(22) Walcarius, A. Zeoliti-modified electrodes in electroanalytical chemistry. *Anal. Chim. Acta* **1999**, *384*, 1–16.
(23) Tonle, I. K.; Ngameni, E.; Walcarius, A. From clay- to organoclay-film modified electrodes: tuning charge selectivity in ion exchange voltammetry. *Electrochim. Acta* **2004**, *49*, 3435–3443.
(24) Mbindyo, J.; Zhou, L. P.; Zhang, Z.; Stuart, J. D.; Rusling, J. F. Detection of chemically induced DNA damage by derivative square wave coltammetry. *Anal. Chem.* **2000**, *72*, 2059–2065.
(25) Laviron, E. Adsorption, autoinhibition and autocatalysis in polarography and in linear potential sweep voltammetry. *Electroanal. Chem. Inter. Electrochem.* **1974**, *52*, 355–393.
(26) Anson, F. C. Evidence for adsorption of cobale(III)−(ethylenedinitrilo) tetraacetate at platinum electrodes. *Anal. Chem.* **1964**, *36*, 520–523.
(27) Watkins, P. J. A study in the use of an extrapolation method to find the equilibrium potential for certain ion-selective electrodes. *Electroanalysis* **1997**, *9*, 85–86.

Received for review April 22, 2010. Revised manuscript received July 8, 2010. Accepted July 13, 2010. This research is supported by the National Nature Science Foundation of China (No. 20805035 and 90817103).